

## INNOVATIVE TECHNOLOGIES OF OIL AND GAS

### EXPERIMENTAL STUDY ON LOGGING EVALUATION OF MATRIX MINERAL MODULUS OF TIGHT SANDSTONE RESERVOIR

Maoxian Pu 

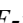
*Porosity has an important influence on the elastic properties of tight sandstone. Using acoustic models to study the matrix mineral modulus of tight sandstone reservoirs can provide an important reference for tight sandstone reservoir evaluation. In this paper, taking tight sandstone as an example, starting from the microscopic pore scale and considering the heterogeneity of the rock skeleton, the effect of the effective stress coefficient of porosity ( $n$ ) on the elastic properties of tight sandstone was discussed. In addition, the acoustic model was used to construct the calculation method of the matrix mineral shear modulus. The research results showed that the porosity disturbance model can better describe the change law of the elastic properties of the tight sandstone. As the value of  $n$  decreases from 1 to 0, the bulk modulus ( $K_\phi$ ) of the unencapsulated rock gradually decreases. In the process of increasing from  $n=0$  to  $n=4$ , the rock  $K_{ud}$  has a slight increase trend. The fluid pressure does not produce a reverse stress effect on the movement of the rock pore boundary, that is, the fluid pressure does not have any effect on the change of the rock porosity. When  $n>0$ , the pore fluid pressure will affect the movement of the rock pore boundary to a certain extent. When the porosity disturbance is not considered, the  $K_\phi$  value of the formation rock will be overestimated. The  $K_o$  of tight sandstone can be obtained using Gassmann fluid substitution equation. The calculation results of modulus parameters accord with the internal mineral composition and structural characteristics of tight sandstone, which shows the effectiveness of the method.*

**Keywords:** porosity, bulk modulus, shear modulus, tight sandstone, well logging evaluation.

#### 1. Introduction

There is a close relationship between the elastic properties of formation rocks and porosity [1-4]. The elastic properties of rocks mainly include bulk modulus ( $K$ ), shear modulus ( $\mu$ ), matrix mineral bulk modulus ( $K_\phi$ ) and matrix mineral shear modulus ( $\mu_\phi$ ). The predecessors have done a lot of research on rock elastic properties and petrophysical parameters [5-9]. These studies can well describe the relationship between porosity and rock elastic properties. From the perspective of rock mass deformation, it can be used to describe the change law of porosity in the process of rock deformation [10-12]. Gassmann's theoretical equation and Biot's theoretical equation can better describe the relationship between the porosity and elastic properties of poroelastic rocks, but these theoretical equations assume that the rock skeleton is a homogeneous medium at the pore scale level [13-17].

---

School of Petroleum Engineering, China University of Petroleum (East China), Qingdao, China. *Corresponding author:* Maoxian Pu . E-mail: pangde11125@163.com. Translated from *Khimiya i Tekhnologiya Topliv i Masel*, No. 1, pp. 76–79, January–February, 2024.

0009-3092/24/6001-0088 © 2024 Springer Science+Business Media, LLC

In fact, the rock skeleton contains different types of pores, and the pores contain fluid components; therefore, during the stress loading process, different pore types have a certain degree of influence on the effective stress of the rock [18-20]. The effective stress acting on the rock is affected by the combined action of confining pressure (environmental stress) and pore pressure [21, 22]. Taking into account the non-uniformity of the rock skeleton of the pore-scale layer, the effective stress coefficient of porosity ( $n$ ) is often used to adjust the proportion between them, so as to better describe the influence of porosity disturbance on the elastic properties of rock [23-26].

Both the bulk modulus of rock matrix mineral  $K_o$  and the matrix mineral shear modulus  $\mu_o$  represent the important mechanical properties of underground pore elastic rock media, reflecting the rock mechanical properties under the conditions of interaction of various minerals in the rock [27-29]. Its accurate evaluation or estimation is of great significance to the inversion of pore and fracture morphology, oil and gas prediction, and reservoir inversion. But in fact, the precise acquisition of these parameters is almost unrealistic. Therefore, a variety of methods for predicting the modulus of rock matrix minerals have emerged. These prediction methods mainly include: prediction methods based on Gassmann's fluid substitution theory, differential equivalent medium theory prediction methods, adaptive matrix mineral modulus extraction methods, and mineral component content estimation methods [25-30]. The above methods can roughly estimate the mineral modulus of the rock matrix, but there are often problems with many undetermined parameters. As a result, when different calculation methods are used to predict the rock matrix mineral modulus of the same formation, the results may have large deviations. Finally, the reliability of the calculation method is reduced.

In this paper, taking tight sandstone as an example, starting from the microscopic pore scale and considering the heterogeneity of the rock skeleton, the effect of the effective stress coefficient of porosity ( $n$ ) on the elastic properties of tight sandstone was discussed. In addition, the acoustic model was used to construct the calculation method of the matrix mineral shear modulus. This study can provide a reference for logging evaluation of rock elastic properties of tight sandstone reservoirs.

## 2. Materials and methods

**Materials.** In this paper, the deep tight sandstone with a buried depth of more than 5000 m in area A has been tested for physical properties and undrained uniaxial acoustics. The sample size is 25×50 mm. Acoustic testing equipment includes three-axis chamber, computer and oscilloscope. The ultrasonic transmitting transducer and the ultrasonic receiving transducer are installed in the three-axis room, the frequency of which is 1MHz; the type of oscilloscope is Philips digital storage oscilloscope. In addition, the internal mineral components of tight sandstone are mainly quartz, feldspar and lithic debris. The average density of the rock is 2.41 g/cm<sup>3</sup>, and the average porosity is 9%.

**Porosity perturbation method.** According to Biot theory, the rock porosity change  $\Delta\eta$  can be expressed by the following Equation according to the rock skeleton ( $(\bar{u}_{j,j}^s)$ ) and the volume strain of pore fluid ( $(\bar{u}_{j,j}^f)$ ):

$$\eta - \eta_0 = \delta_s \bar{u}_{j,j}^s - \delta_f \bar{u}_{j,j}^f, \quad (1)$$

where,  $\delta_s$  and  $\delta_f$  are dimensionless coefficients, which can be expressed as Equations:

$$\delta_s = (1 - \eta_0) \delta_{Ks} \frac{\eta_0 M'}{K_f}, \quad (2)$$

$$\delta_f = (1 - \eta_0) \delta_{Ks} \frac{\eta_0 M'}{K_s}, \quad (3)$$

where  $K_f$  is the fluid bulk modulus, GPa;  $\delta_{Ks}$  is a modified Biot volume coefficient,  $\delta_{Ks} = (\alpha - \eta_0) / (1 - \eta_0)$ ;  $M'$  can be expressed by equation

$$M'^{-1} = M^{-1} - \frac{\alpha - \eta_0}{K_s} (1 - n). \quad (4)$$

$M^{-1}$  can be expressed as:  $M^{-1} = \eta_0 / K_f + (\alpha - \eta_0) / K_s$ , and further, the bulk modulus ( $K_{ud}$ ) of undrained rock can be expressed as:

$$K_{ud} = K_o + \alpha(\alpha - (1 - n)(\alpha - \eta_0)) M^{-1}. \quad (5)$$

When  $n$  takes 1 in Equation (5), the effect of porosity disturbance is not considered at this time, and the equation can be simplified to Equation (6), which is the expression of Gassmann's non-drained bulk modulus.

$$K_{ud} = K_o + \alpha^2 M. \quad (6)$$

**Acoustic model.** Gassman equations (Equations (7)-(8)) can generally be used to construct the vertical and horizontal wave velocity of the rock under the condition of formation saturated with water [31-33]. The density of rock under formation conditions can be expressed by Equation (9) according to the density of the rock skeleton  $\rho$ , the density of saturated fluid  $\rho_{fl}$  and the porosity  $\phi$ .

$$V_p = \sqrt{\frac{K + \frac{4}{3}\mu}{\rho}}, \quad (7)$$

$$V_s = \sqrt{\frac{\mu}{\rho}}, \quad (8)$$

$$\rho = (1 - \phi)\rho_{ma} + \phi\rho_{fl}, \quad (9)$$

where  $V_p$  and  $V_s$  are the longitudinal wave velocity and shear wave velocity of the rock under the saturated formation condition, km/s;  $K$  and  $\mu$  are the bulk modulus and shear modulus of the rock under the formation saturated condition, GPa.

According to (8) and (9), we can get:

$$\frac{V_p}{V_s} = \sqrt{\frac{k + \frac{4}{3}\mu}{\mu}}. \quad (10)$$

According to the Biot – Gassmann theory, the Biot coefficient  $\alpha$  is introduced. At this time, the rock bulk modulus  $K$  and shear modulus  $\mu$  can be expressed as:

$$K = K_o(1 - \alpha) + \alpha^2 M, \quad (11)$$

$$\mu = \mu_o(1 - \alpha), \quad (12)$$

$$\frac{1}{M} = \frac{\alpha - \phi}{K_o} + \frac{\phi}{k_{fl}}, \quad (13)$$

where  $K_o$  and  $\mu_o$  are the bulk modulus and shear modulus of the matrix mineral, respectively, GPa;  $k_{fl}$  is the bulk modulus of the saturated fluid, which is calculated by Wood's equation, GPa.

The Biot coefficient can be determined according to Equation (14):

$$\alpha = 1 - \frac{\rho_d(V_{pd}^2 - 4V_{sd}^2/3)}{K_o}, \quad (14)$$

where  $\rho_d$  is the dry rock density, g/cm<sup>3</sup>;  $V_{pd}$  and  $V_{sd}$  are the dry rock longitudinal wave velocity and dry rock shear wave velocity, km/s, respectively.

Substituting Equation (11)-(12) into Equation (11), we can get equation:

$$\left(\frac{V_p}{V_s}\right)^2 = \frac{4}{3} + \frac{K_o}{\mu_o} + \frac{\alpha^2 M}{\mu_o(1 - \alpha)}. \quad (15)$$

Equation (15) shows that the wave velocity ratio ( $V_p/V_s$ ) is a function of the introduced Biot coefficient  $\alpha$ . The satisfied relationship between the vertical and horizontal wave velocities of the test rock samples is as equation:

$$V_s = V_p G \gamma (1 - \phi)^n, \quad (16)$$

where  $\gamma$  is the  $V_s/V_p$  ratio of the matrix mineral, dimensionless;  $G$  is the fitting parameter, dimensionless.

According to equation (7)-(8) and Equation (16), we can get equation:

$$\mu = \frac{\mu_o G^2 (1 - \phi)^{2n} k}{K_o + 4\mu_o [1 - G^2 (1 - \phi)^{2n}] / 3}. \quad (17)$$

Substituting Equation (17) into Equation (10), Equation (18) can be obtained:

$$\left(\frac{V_p}{V_s}\right)^2 = \frac{4}{3} + \frac{K_o}{\mu_o G^2 (1-\phi)^{2n}} + \frac{4[1-G^2(1-\phi)^{2n}]}{3G^2(1-\phi)^{2n}}. \quad (18)$$

Equation (18) shows that the ratio of the wave velocity of the vertical and horizontal waves of the rock is a function of the porosity of the rock, thus realizing the effective replacement of the Biot coefficient by the porosity. The value range of  $n$  is 0-1. The value of  $n$  is related to factors such as rock type, rock consolidation degree and mineral content. For the deep tight sandstone in this study,  $n$  is taken as 1. In this case, equation (18) can be transformed into equation:

$$\left(\frac{V_p}{V_s}\right)^2 = \frac{3K_o + 4\mu_o}{3\mu_o G^2 (1-\phi)^2}. \quad (19)$$

It can be seen from Equation (19) that  $(V_p/V_s)^2$  and  $(1-\phi)^2$  satisfy a linear relationship. For parameter  $G$ , its value range is 0-1, and the value should also satisfy Equation (10).

According to Equation (19), the corresponding slope can be obtained by using the linear relationship between  $(V_p/V_s)^2$  and  $(1-\phi)^2$ .  $K_o$  can be obtained according to the linearization method derived from the Gassmann fluid substitution equation [34-36]. The relationship between rock porosity  $\phi$  and equivalent volumetric compressibility  $\beta_v$  is shown in equations:

$$\phi = A\beta_v - B, \quad (20)$$

$$A = \left(\frac{1}{\beta_f} + \frac{C}{\beta_s}\right), \quad (21)$$

$$B = \beta_s \left(\frac{1}{\beta_f} + \frac{C}{\beta_s}\right), \quad (22)$$

where  $\beta_f$  is the compressibility of the saturated fluid,  $10^{-3}$ GPa;  $\beta_s$  is the mineral compressibility of the rock matrix,  $10^{-3}$ GPa;  $C$  is the rock pore structure parameter.

$\beta_v$  can be expressed by Eq. (23). Comparing Eq. (21) and Eq. (22), the expression of the bulk modulus of rock matrix minerals can be obtained, as shown in equation (24).

$$\beta_v = \frac{1}{\rho_s(V_p^2 - 4V_s^2 / 3)}, \quad (23)$$

$$\mu_o = A/B. \quad (24)$$

### 3. Results and analysis

**Rock bulk modulus ( $K_s$ ) and matrix mineral bulk modulus ( $K_o$ ).** It can be seen from Figure 1 that when the value of  $n$  is in the range of 0-4,  $K_{ud} > K_s$ . In the process of increasing from  $n=0$  to  $n=4$ , the rock  $K_{ud}$  has a slight increase trend. For  $K_{ud}$  and  $K_o$ , when  $n=0$ , the fluid pressure does not produce a reverse stress on the movement of the rock pore boundary, that is, the fluid pressure does not have any effect on the change of rock porosity. At this time,  $K_{ud} = K_o$ . When  $n > 0$ , the pore fluid pressure will affect the movement of the rock pore boundary to a certain extent. At this time,  $K_{ud} > K_o$  (**Figure 1**).

**Relationship between rock bulk modulus  $K_\phi$  and porosity.** It can be seen from **Figure 2** that in the range of  $n=0$  to 1, the 6 sets of test data basically fall on the curve in the range of  $n=0.4$  to 0.8, and the average value of  $n$  is about 0.6, indicating that the porosity perturbation equation can more accurately describe the changes in the elastic properties of the target rock.

The pore compressibility coefficient ( $C_\phi$ ) of unencapsulated rock is related to the rock pore compressibility coefficient ( $C_{pc}$ ) under confining pressure and the rock pore compressibility coefficient ( $C_{pp}$ ) under pore pressure conditions, which can be expressed as:  $C_\phi = C_{pc} - C_{pp}$ . Then we can get:

$$C_\phi = C_s \left(1 + \frac{1}{\eta_0} (1-n) \frac{\delta K_s}{1 - \delta K_s}\right). \quad (25)$$

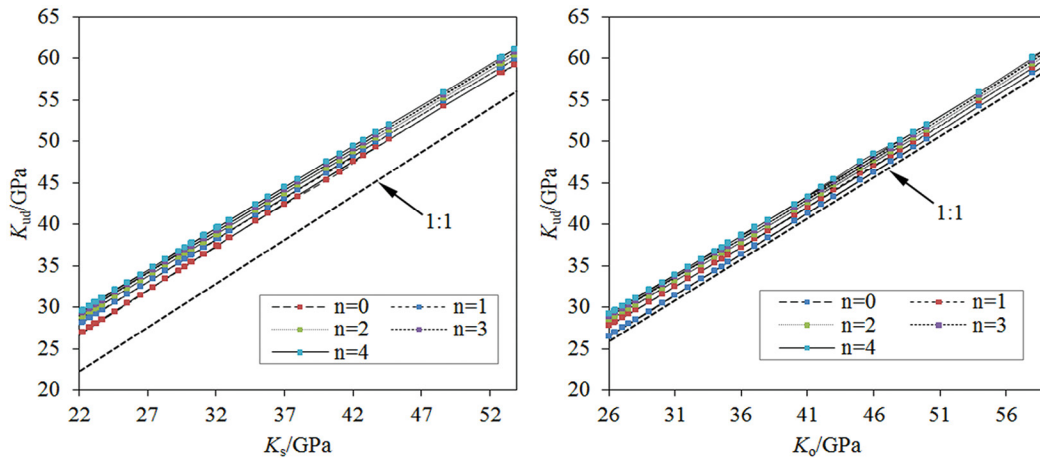


Fig. 1. Relationship between  $K_{ud}$  and  $K_s$  and  $K_0$

Correspondingly, the pore bulk modulus of unencapsulated rock  $K_\phi = C_\phi^{-1}$ . When  $n$  is 1, the porosity disturbance is not considered, at this time  $K_\phi = K_s$ . The results of the triaxial mechanics test show that the  $n$  value of the formation rock is  $<1$ , therefore,  $K_\phi < K_s$ . As the value of  $n$  gradually decreases from 1 to 0, the calculated rock  $K_\phi$  gradually decreases.

Since the six sets of mechanical test data in Fig. 2 showed that the  $n$  value of tight sandstone in this area is mainly distributed in the range of 0.4 to 0.8, the average value is 0.6. Therefore, the intersection of the rock  $K_\phi$  and the porosity of the formation rock calculated under the three conditions of  $n=0.4$ , 0.6 and 0.8 was analyzed (Figure 3). It can be seen that  $K_\phi$  has a good negative correlation with rock porosity, the data at the two ends have a slower trend, and the central data has a steeper trend. For the case where  $n$  takes an average value of 0.6, as the porosity of the formation rock increases from about 2.1% to 4.7%, the corresponding rock  $K_\phi$  decreases from about 24 GPa to 6.2 GPa. Porosity has a significant influence on the rock  $K_\phi$ . When the porosity disturbance is not considered, the  $K_\phi$  value of the formation rock will be overestimated.

**Determination of the shear modulus of matrix minerals  $K_0$ .** The lithology of the studied tight sandstone samples is mainly feldspar lithic sandstone, and the tight particle contact relationship of the tight sandstone can be seen under the scanning electron

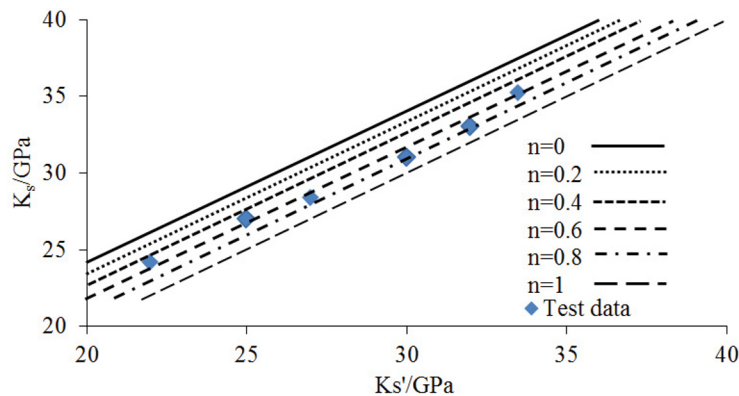


Fig. 2. Relationship between rock  $K_s$  and  $K_s'$

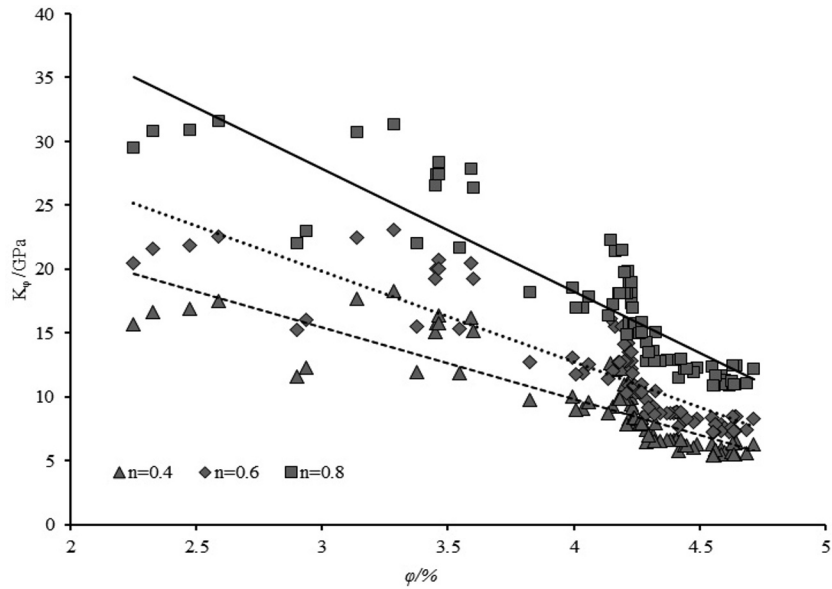


Fig. 3. Relationship between  $K_0$  and porosity of tight sandstone in the target layer

microscope (Figure 4). The permeability of the samples is less than 1mD, which belongs to tight sandstone. Under the saturated condition of each sample, the measured longitudinal wave velocity is greater than the transverse wave velocity. For samples with relatively high porosity and relatively low density, the measured longitudinal wave velocity is relatively small. Because the main mineral components of the sandstone are quartz, plagioclase, calcite, pyrite and clay minerals. Moreover, minerals such as plagioclase, calcite and pyrite have high  $K_0$  values. Minerals such as quartz and pyrite have high  $\mu_0$  values. Therefore, the mineral composition and microscopic contact patterns in the rock are the important reasons for the high  $k_0$  and  $\mu_0$  values of the tight sandstone in this formation. At the same time, the burial depth of the tight sandstone formation is relatively large, and the vertical effective stress can reach 66 MPa, so the matrix mineral modulus is relatively high or the compressibility is relatively small.

Firstly, the  $\beta_v$  of each group of samples is obtained according to Equation (17). From Equation (14), it can be known that  $\beta_v$  and the porosity of each group of samples satisfy a linear relationship. A and B are calculated according to the slope, and according to Equation (18), the matrix mineral bulk modulus of the sandstone of the formation is calculated as  $K_0=73$  GPa. There is a very

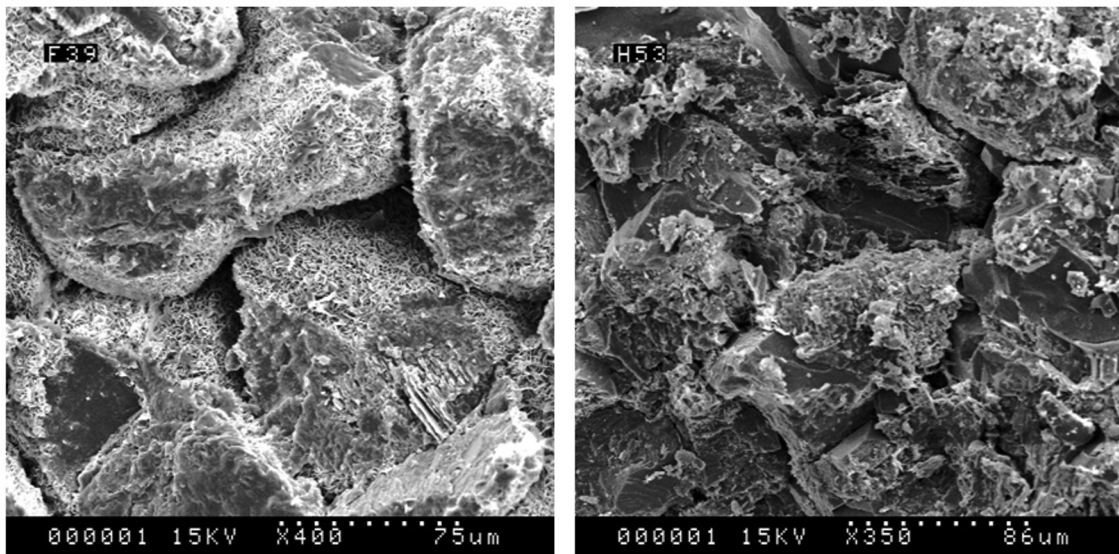
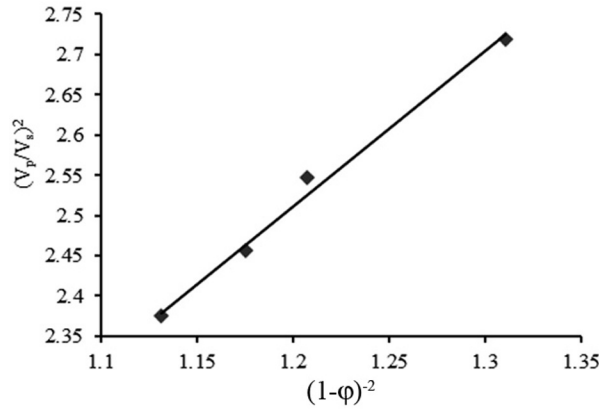


Fig. 4. Tight particle contacts relationship of tight sandstone



**Fig. 5. Relationship between  $(V_p/V_s)^2$  and  $(1-\phi)^2$  of tight sandstone samples**

good linear relationship between  $(V_p/V_s)^2$  and  $(1-\phi)^2$  (**Figure 5**). Furthermore, according to the slope of the curve,  $K_o$  and  $G$  values, the shear modulus of the rock matrix mineral of the formation can be calculated as  $\mu_o=55$  GPa.

The  $K_o$  and  $\mu_o$  values of deep-seated tight sandstone samples determined by this method can be compared with the results of mineral composition estimation. The sandstone of this formation is dense, and the micrograph shows that most of the grains are in contact with points, lines, and bumps. The cuttings are mainly flint cuttings, in addition to some clay cuttings, volcanic cuttings and quartz cuttings. Moreover, the interstitial material is calcite, which is plaque-like, with continuous and granular cementation, and is evenly distributed in the intergranular pores. The siliceous material is occasionally enlarged by quartz, and a small amount of secondary pyrite can be seen at the same time. The clay is mainly distributed among the debris and is in the form of a mud film. On the whole, the calculated results are consistent with the mineral composition and structure of tight sandstones, indicating the reliability of the method in this paper.

#### 4. Conclusions

In this paper, taking tight sandstone as an example, starting from the microscopic pore scale and considering the heterogeneity of the rock skeleton, the effect of the effective stress coefficient of porosity ( $n$ ) on the elastic properties of tight sandstone was discussed. In addition, the acoustic model was used to construct the calculation method of the matrix mineral shear modulus.

The research results showed that the porosity disturbance model can better describe the change law of the elastic properties of the tight sandstone. As the value of  $n$  decreases from 1 to 0, the bulk modulus ( $K_\phi$ ) of the unencapsulated rock gradually decreases. In the process of increasing from  $n=0$  to  $n=4$ , the rock  $K_{ud}$  has a slight increase trend.

The fluid pressure does not produce a reverse stress effect on the movement of the rock pore boundary, that is, the fluid pressure does not have any effect on the change of the rock porosity. When  $n>0$ , the pore fluid pressure will affect the movement of the rock pore boundary to a certain extent. When the porosity disturbance is not considered, the  $K_\phi$  value of the formation rock will be overestimated.

The  $K_o$  of tight sandstone can be obtained using Gassmann fluid substitution equation. The calculation results of modulus parameters accord with the internal mineral composition and structural characteristics of tight sandstone, which shows the effectiveness of the method.

#### Acknowledgements

The author hope to show sincere thanks to the engineers who have contributed this work.

#### REFERENCES

1. Pang, Y.M., Guo, X.W., Han, Z.Z., et al. (2019) Mesozoic-Cenozoic denudation and thermal history in the Central Uplift of the South Yellow Sea basin and the implications for hydrocarbon systems: Constraints from the CSDP-2 borehole. *Marine and Petroleum Geology*, 99, 355-369.

2. Yang, R., Fan, A., Han, Z., et al. (2017) Lithofacies and origin of the late triassic muddy gravity-flow deposits in the Ordos Basin, Central China. *Marine and Petroleum Geology*. 85, 194-219.
3. Berryman, J., Pride, S., Wang, H. (2002) A differential scheme for elastic properties of rocks with dry or saturated cracks. *Geophys. Journal. International*. 151, 597-611.
4. Russell, B., Hedlin, K. (2003) Fluid-property discrimination with AVO: a Biot-Gassman perspective. *Geophysics*. 68(1), 29-39.
5. Guan, X., Meng, Q., Wang, B. et al. (2023) Description of Formations Fault Activity Characteristics and Genesis Mechanism Using of Paleogeomorphic Restoration Techniques. *Chem Technol Fuels Oils*. 59, 647-660.
6. Myung, W. (2003) Velocity ratio and its application to predicting velocities. *U.S. Geological Survey Bulletin*. 13, 1-15.
7. Krief, M., Garat, J., Stellingwerff, J., et al. (1990) A petrophysical interpretation using the velocities of P and S waves (full-waveform sonic). *The Log Analyst*. 31, 355- 369.
8. Ma, Z. (2008) Experimental study on Biot coefficient and rock elastic modulus. *Oil and Gas Geology*. 29(1), 135-140.
9. Qiu, X., Liu, C., Mao, G., et al. (2014) Late Triassic tuff intervals in the Ordos basin, Central China: Their epositional, petrographic, geochemical characteristics and regional implications. *Journal of Asian Earth Sciences*. 80, 148-160.
10. Wang, S.J., Li, X.P., Schertl, H.P., et al. (2019) Petrogenesis of early cretaceous andesite dykes in the Sulu orogenic belt, eastern China. *Mineralogy and Petrology*. 113(1), 77-97.
11. Zhao, N., Wang, L., Sima, L.Q., et al. (2022) Understanding stress-sensitive behavior of pore structure in tight sandstone reservoirs under cyclic compression using mineral, morphology, and stress analyses. *Understanding stress-sensitive behavior of pore structure in tight sandstone reservoirs under cyclic compression using mineral, morphology, and stress analyses*. 218, 110987.
12. Myung, W. (2002) Biot-Gassman theory for velocities of gas hydrate-bearing sediments. *Geophysics*. 67(6), 1711-1719.
13. Zhu, J., Fang, Z., Li, Y. (2014) Petrophysical characteristics and application of Zhuhai Formation in W area. *Mineralogy and Petrology*. 34(2), 113-120.
14. Si, X., Cao, Q., Ji, W. (2014) Tight sandstone reservoir characteristics and influencing factors of Shuixigou Group in Taipei Sag, Turpan-Hami Basin. *Mineralogy and Petrology*. 34(4), 93-101.
15. Wang, C., Liu, L., Xiao, P., et al. (2014) Geochemical and geochronologic constraints for paleozoic magmatism related to the orogenic collapse in the qimantagh-south altyn region, Northwestern China. *Lithos*. 202-203, 1-20.
16. Liu, L., Kang, L., Cao, Y., et al. (2015) Early paleozoic granitic mag matism related to the processes from subduction to collision in south Altyn, NW China. *Science China Earth Sciences*. 58(9), 1513-1522.
17. Liu, Y., Hu, W., Cao, J., et al. (2017) Diagenetic constraints on the heterogeneity of tight sandstone reservoirs: a case study on the upper Triassic Xujiahe formation in the Sichuan Basin, Southwest China. *Marine and Petroleum Geology*. 92, 650-669.
18. Jiang, L., Sainoki, A., Mitri, H., et al. (2016) Influence of fracture-induced weakening on coal mine gateroad stability. *International Journal of Rock Mechanics and Mining Sciences*. 88, 307-317.
19. Kate, H. (1975) Vp/Vs anomalies in dilatants rock samples. *Pure and Applied Geophysics*. 113, 1-21.
20. Lasaga, A. (1984) Chemical kinetics of water-rock interactions. *Journal of Geophysical Research*. 89(B6), 4009-4025.
21. Zhang, X., Feng, Q., Sun, P., et al. (2010) Characteristics of high gamma ray reservoir of Yanchang formation in Ordos Basin. *Chinese Journal of Geophysics*. 53(1), 205-213.
22. Xiao, D., Lu, Z., Jiang, S., Lu, S. (2016) Comparison and integration of experimental methods to characterize the full-range pore features of tight gas sandstone-A case study in Songliao Basin of China. *Journal of Natural Gas Science and Engineering*. 34, 1412-1421.
23. Shanley, K., Cluff, R. (2015) The evolution of pore-scale fluid-saturation in low permeability sandstone reservoirs. *AAPG Bulletin*. 99, 1957-1990.
24. Pittman E. (1992) Relationship of porosity and permeability to various parameters derived from mercury injection capillary pressure curves for sandstone. *AAPG Bulletin*. 76, 191-198.



25. Loucks, R., Reed, R., Ruppel, S., Jarvie, D. (2009) Morphology, genesis, and distribution of nanometer-scale pores in siliceous mudstones of the Mississippian Barnett shale. *J Sediment Res.* 79, 848-861.
26. Chen, Z., Li, Q., Liu, M., et al. (2021) Uranium mineralization formed through multi-stage superposition: Case of the Qianjiadian deposit in Songliao Basin, China. *Energy Geoscience.* 2(1), 2021, 32-40.
27. Morozov, V.P., Jin, Z., Liang, X., et al. (2021) Comparison of source rocks from the Lower Silurian Longmaxi Formation in the Yangzi Platform and the Upper Devonian Semiluksk Formation in East European Platform. *Energy Geoscience.* 2(1), 63-72.
28. Wang, G., Chang, X., Yin, W., et al. (2017) Impact of diagenesis on reservoir quality and heterogeneity of the upper Triassic Chang 8 tight oil sandstones in the Zhenjing area, Ordos Basin, China. *Marine and Petroleum Geology.* 83, 84-96.
29. Yang, R., Jin, Z., Van Loon, A., et al. (2017) Climatic and tectonic controls of lacustrine hyperpycnite origination in the late triassic Ordos Basin, Central China: implications for unconventional petroleum development. *AAPG Bulletin.* 101(01), 95-117.
30. Asante-Okyere, S., Ziggah, Y.Y., et al. (2021) Improved total organic carbon convolutional neural network model based on mineralogy and geophysical well log data. *Unconventional Resources.* 1, 1-8.
31. Vafaie, A., Kivi, I., Moallemi, S., et al. (2021) Permeability prediction in tight gas reservoirs based on pore structure characteristics: A case study from South Western Iran. *Unconventional Resources.* 1, 9-17.
32. Kirmani, F., Raoof Gholami, A., Haidar, M., et al. (2021) Analyzing the effect of steam quality and injection temperature on the performance of steam flooding. *Energy Geoscience.* 2(1), 83-86.
33. Nieves, L., Elyseu, F., Goulart, S., et al. (2021) Use of fly and bottom ashes from a thermoelectrical plant in the synthesis of geopolymers: Evaluation of reaction efficiency, *Energy Geoscience.* 2(2), 167-173.
34. Katz, B., Gao, L., Little, J., et al. (2021) Geology still matters - Unconventional petroleum system disappointments and failures. *Unconventional Resources.* 1, 18-38.
35. Qiu, X., Liu, C., Mao, G., et al. (2015) Major, trace and platinum-group element geochemistry of the upper triassic non-marine hot shales in the Ordos Basin, central china. *Applied Geochemistry.* 53, 42-52.
36. Wang, D., Shao, L., Li, Z., et al. (2016) Hydrocarbon generation characteristics, reservoir performance and preservation conditions of continental coal measure shale gas: a case study of mid-jurassic shale gas in the Yan'an formation, Ordos Basin. *Journal of Petroleum Science and Engineering.* 145, 609-628.